JCI The Journal of Clinical Investigation

PPARβ/δ affects pancreatic β cell mass and insulin secretion in mice

José Iglesias, Sebastian Barg, David Vallois, Shawon Lahiri, Catherine Roger, Akadiri Yessoufou, Sylvain Pradevand, Angela McDonald, Claire Bonal, Frank Reimann, Fiona Gribble, Marie-Bernard Debril, Daniel Metzger, Pierre Chambon, Pedro Herrera, Guy A. Rutter, Marc Prentki, Bernard Thorens, Walter Wahli

J Clin Invest. 2012;122(11):4105-4117. https://doi.org/10.1172/JCI42127.

Research Article **Metabolism**

PPARβ/δ protects against obesity by reducing dyslipidemia and insulin resistance via effects in muscle, adipose tissue, and liver. However, its function in pancreas remains ill defined. To gain insight into its hypothesized role in β cell function, we specifically deleted *Pparb/d* in the epithelial compartment of the mouse pancreas. Mutant animals presented increased numbers of islets and, more importantly, enhanced insulin secretion, causing hyperinsulinemia. Gene expression profiling of pancreatic β cells indicated a broad repressive function of PPARβ/δ affecting the vesicular and granular compartment as well as the actin cytoskeleton. Analyses of insulin release from isolated PPARβ/δ-deficient islets revealed an accelerated second phase of glucose-stimulated insulin secretion. These effects in PPARβ/δ-deficient islets correlated with increased filamentous actin (F-actin) disassembly and an elevation in protein kinase D activity that altered Golgi organization. Taken together, these results provide evidence for a repressive role for PPARβ/δ in β cell mass and insulin exocytosis, and shed a new light on PPARβ/δ metabolic action.

PPARβ/δ affects pancreatic β cell mass and insulin secretion in mice

José Iglesias,[1,2] Sebastian Barg,[3,4] David Vallois,[1] Shawon Lahiri,[1] Catherine Roger,[1] Akadiri Yessoufou,[1] Sylvain Pradevand,[1] Angela McDonald,[4] Claire Bonal,[5] Frank Reimann,[6] Fiona Gribble,[6] Marie-Bernard Debril,[1] Daniel Metzger,[7] Pierre Chambon,[7] Pedro Herrera,[5] Guy A. Rutter,[4] Marc Prentki,[2] Bernard Thorens,[1] and Walter Wahli[1]

[1]Center for Integrative Genomics, National Research Center Frontiers in Genetics, University of Lausanne, Lausanne, Switzerland. [2]Montreal Diabetes Research Center and University of Montreal Hospital Research Centre (CRCHUM), and Departments of Nutrition and Biochemistry, University of Montreal, Montreal, Quebec, Canada. [3]Department of Medical Cell Biology, Uppsala University, Uppsala, Sweden. [4]Section of Cell Biology, Division of Medicine, Imperial College London, London, United Kingdom. [5]Department of Genetic Medicine and Development, University of Geneva Medical School, Geneva, Switzerland. [6]Cambridge Institute for Medical Research, Cambridge, United Kingdom. [7]Institut de Génétique et de Biologie Moléculaire et Cellulaire, INSERM 964, Université de Strasbourg, Illkirch, France.

PPARβ/δ protects against obesity by reducing dyslipidemia and insulin resistance via effects in muscle, adipose tissue, and liver. However, its function in pancreas remains ill defined. To gain insight into its hypothesized role in β cell function, we specifically deleted *Pparb/d* in the epithelial compartment of the mouse pancreas. Mutant animals presented increased numbers of islets and, more importantly, enhanced insulin secretion, causing hyperinsulinemia. Gene expression profiling of pancreatic β cells indicated a broad repressive function of PPARβ/δ affecting the vesicular and granular compartment as well as the actin cytoskeleton. Analyses of insulin release from isolated PPARβ/δ-deficient islets revealed an accelerated second phase of glucose-stimulated insulin secretion. These effects in PPARβ/δ-deficient islets correlated with increased filamentous actin (F-actin) disassembly and an elevation in protein kinase D activity that altered Golgi organization. Taken together, these results provide evidence for a repressive role for PPARβ/δ in β cell mass and insulin exocytosis, and shed a new light on PPARβ/δ metabolic action.

Introduction

High plasma glucose levels due to insulin resistance and inadequate insulin production characterize type 2 diabetes. Generally considered an adult illness, it is now often diagnosed in teenagers in parallel with rising obesity rates. Type 2 diabetes is a multigenic disease, and several genome-wide association studies have identified many novel loci, most seeming to influence β cell capacity to enhance insulin secretion in response to increased insulin resistance or body weight (1, 2). Many of the identified insulin secretory defects remain poorly understood at the molecular level, especially the decline in β cell mass and function.

Mechanisms regulating adult β cell mass include proliferation of preexisting β cells (3) and β cell neogenesis from ductal precursor cells (4). Tight regulation of β cell mass is required for preserving insulin secretion capacity over a lifetime. In fact, glucose-induced pancreatic β cell expansion supports the notion of existing β cell replication in the adult organism, but the mechanisms of β cell homeostasis and regenerative repair are not well understood.

In rodents, glucose-stimulated insulin secretion (GSIS) exhibits a biphasic pattern characterized by a rapid (5–10 minutes) first-phase release, followed by a second phase of slow, pulsatile release (5, 6). This pattern also occurs in humans (7) and is important for insulin to fulfill its regulatory function (8). The increase of cytoplasmic Ca^{2+} triggered by enhanced circulating glucose levels induces a first-phase release that corresponds to exocytosis of a readily releasable pool (RRP) of insulin-containing granules predocked beneath the cell surface and granules newly recruited that fuse immediately to the plasma membrane (9). A more enduring second-phase release follows, in which new granules are recruited from a reserve pool (RP) by processes referred to as priming (10). Among the molecular mechanisms regulating RRP and RP, the diacylglycerol-activated (DAG-activated) protein Munc13-1 (11) and the GTP-regulated protein Rab3 (12) are involved in granule priming in pancreatic β cells. Furthermore, capacitance measurements and perifusion experiments using cell lines and mouse islets have demonstrated that cytoskeleton regulator proteins also affect priming (13–16). Finally, the p38δ/PKD1 pathway integrates regulation of the insulin secretory capacity and β cell survival (17).

None of the above-mentioned studies have, however, revealed a master regulator that would coordinate glucose sensing and insulin secretion from granule formation to exocytosis. Free fatty acids have complex regulatory roles in insulin secretion (18). Acute treatment of islets with palmitate potentiates GSIS in the β cell, both via intracellular metabolic lipid signaling (19) and the free fatty acid receptor GPR40 (20). Another fatty acid receptor that plays a role in insulin secretion is PPARα (NR1C1). In fact, we showed that pancreatic islet adaptation to fasting is dependent on PPARα transcriptional upregulation of fatty acid oxidation (21). A second PPAR that has been shown to play a role in β cell function is PPARγ (NR1C3) (22). Little is known about PPARβ/δ (NR1C2), the third member of the family. Glucose-induced lipid peroxidation of arachidonic acid and linoleic acid generates endogenous ligand of PPARβ/δ, which induces insulin secretion in INS-1E and rat isolated islets (23). Hence, we hypothesized that the fatty acid receptor PPARβ/δ may play a general regulatory role in these cells. This receptor shows a broad expression pattern and controls processes such as the inflammatory response, cell differentiation, and survival (24–30). So far, PPARβ/δ has been implicated in systemic glucose and lipid homeostasis by its action in nonpancreas tissues. The PPARβ/δ ligand GW501516 reverses meta-

Conflict of interest: The authors have declared that no conflict of interest exists.
Citation for this article: *J Clin Invest.* 2012;122(11):4105–4117. doi:10.1172/JCI42127.

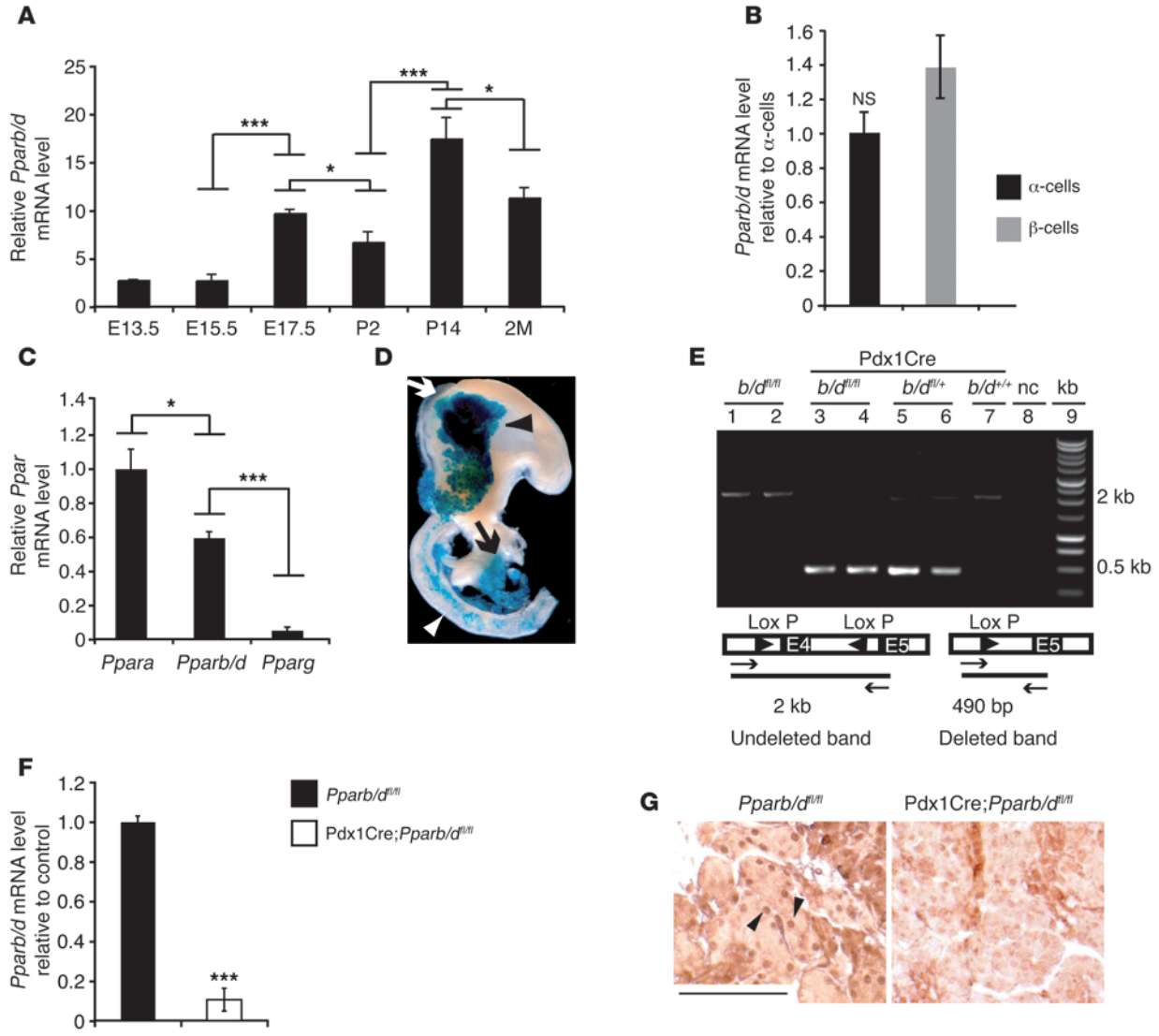

Figure 1

Pparb/d ablation in pancreas. (**A**) Relative *Pparb/d* mRNA expression levels in the pancreas at different stages of fetal and postnatal life ($n = 4$). $^*P < 0.05$; $^{***}P < 10^{-4}$. (**B**) *Pparb/d* mRNA expression levels in pancreatic α- and β-sorted cells from adult mice by FACS ($n = 3$). $^*P < 0.05$; $^{***}P < 10^{-4}$. (**C**) Relative mRNA expression of the 3 PPAR isotypes, *a*, *b/d*, and *g*, in human islets ($n = 3$). $^*P < 0.05$; $^{***}P < 10^{-4}$. (**D**) Cre activity in E15.5 Pdx1Cre;R26R mice revealed by β-gal activity in the Pdx1 expression domain; dorsal (black arrowhead) and ventral (black arrow) pancreas; spleen (white arrow); duodenum (white arrowhead). (**E**) PCR analysis of pancreatic DNA. The 490-bp "deleted" band (lanes 3 and 4) in Pdx1Cre;*Pparb/d*$^{fl/fl}$ mice confirms *Pparb/d* excision. The 2-kb band is from the WT allele (lane 7) or the nondeleted floxed allele (lanes 1 and 2). Both the WT and excised alleles are detected in Pdx1Cre;*Pparb/d*$^{fl/+}$ mice (lanes 5 and 6). nc, negative control; kb, DNA ladder. (**F**) TaqMan analysis of *Pparb/d* mRNA levels in WT and mutated islets ($n = 3$). $^{***}P < 10^{-4}$. (**G**) Detection of PPARβ/δ by immunostaining in cell nuclei of pancreas from E17.5 embryos. In the left panel, a few positive nuclei are indicated by arrowheads as examples. Scale bar: 100 μm.

bolic abnormalities associated with obesity, such as dyslipidemia and insulin resistance, in humans, monkeys, and mice (31–33).

The benefits of PPARβ/δ have been attributed to its induction of genes related to fatty acid oxidation and energy dissipation in adipose tissue and muscle (34, 35). Furthermore, it has been proposed that PPARβ/δ protects GSIS against adverse effects associated with prolonged fatty acid exposure in INS-1E and HIT cells (36, 37). However, its role in vivo remains to be explored. Here, we report the generation and analysis of pancreas-specific *Pparb/d*-null mice, which revealed an unexpectedly broad repressive role for PPARβ/δ on pancreatic β cell proliferation and function.

Results

Pancreatic PPARβ/δ expression. PPARβ/δ expression in mouse pancreas is poorly characterized. However, it is known to occur in rat pancreas from E15.5 in both the endocrine and exocrine compartments (24). We found increased *Pparb/d* mRNA expression during mouse pancreas development (Figure 1A), with levels 3 times higher at E17.5 than at E13.5 and E15.5. At P14, *Pparb/d* mRNA levels had increased 2-fold versus those at P2, but then decreased at 2 months of age after exocrine pancreas expansion. The RNA expression pattern of PPARβ/δ was more similar to that of PPARα than of PPARγ (Supplemental Figure 1, A and B; supplemental material available

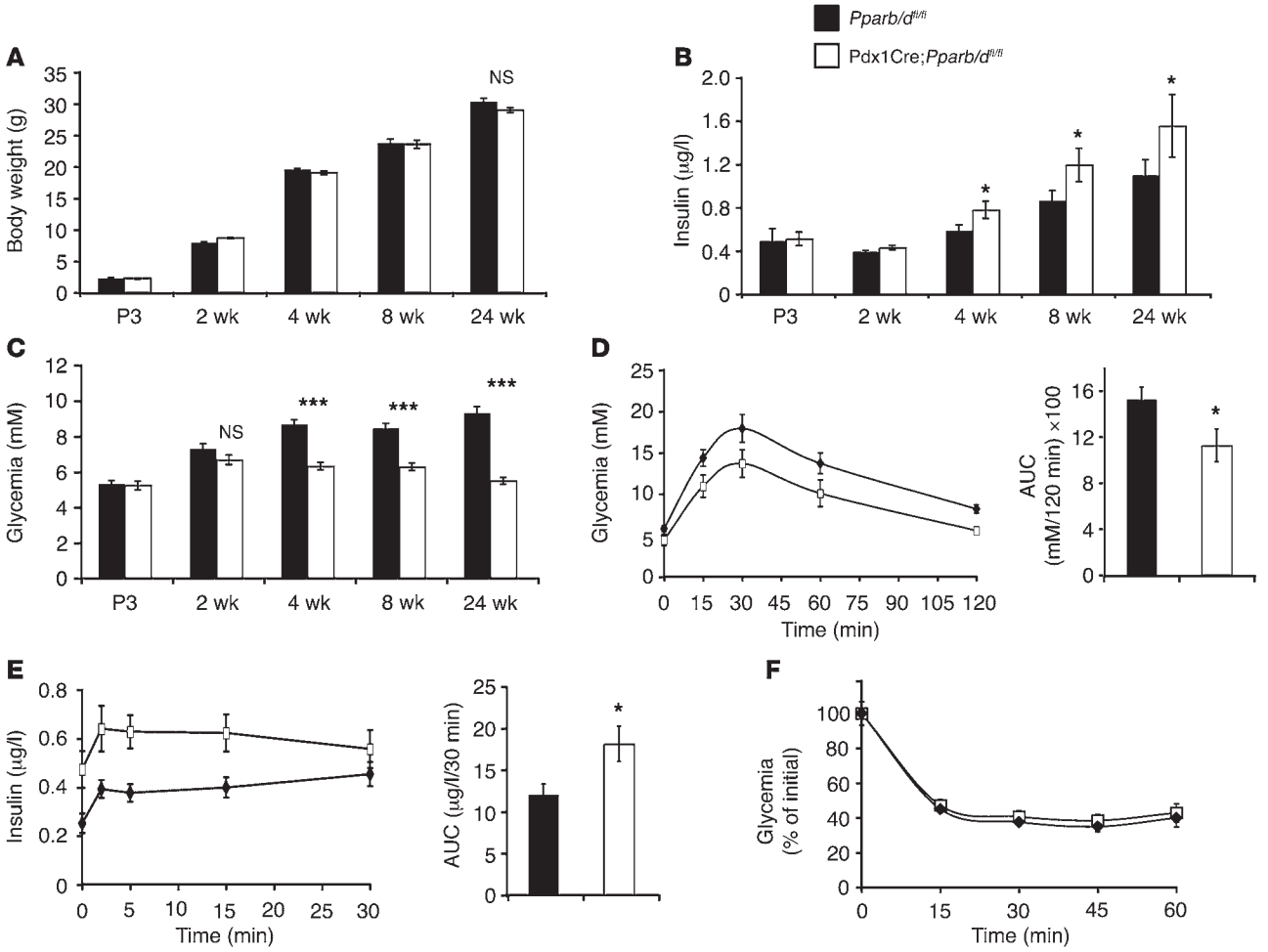

Figure 2

Pparb/d deletion in pancreas results in increased plasma insulin levels. (**A**) Body weight at P3 and weeks 2, 4, 8, and 24 ($n = 20$). (**B**) Fed state plasma insulin levels (P3 and 2, 4, 8, and 24 weeks) ($n = 10–15$). *$P < 0.05$. (**C**) Plasma glucose levels in the same groups of mice as in **A** and **B** ($n = 10–15$). ***$P < 10^{-6}$. (**D**) Left panel: GTT in 12-hour–fasted 8-week-old mice; right panel: AUC ($n = 5$). *$P < 0.05$. (**E**) Left panel: plasma insulin levels in 12-hour–fasted 8-week-old mice; right panel: AUC ($n = 5$). *$P < 0.05$. (**F**) ITT in fed 8-week-old mice ($n = 5$).

online with this article; doi:10.1172/JCI42127DS1). FACS-sorted cells from adult mouse islets showed that PPARβ/δ was expressed in both α and β cells (Figure 1B). PPARβ/δ is also expressed in human islets, although slightly less than PPARα (Figure 1C). Considering the important expression of PPARβ/δ in both mouse and human islets and the whole mouse pancreas (Figure 1C and Supplemental Figure 1C), we concentrated on elucidating its functions in pancreatic β cells.

Deletion of Pparb/d in the pancreas. Deletion of *Pparb/d* or overactivation of PPARβ/δ, specifically in muscle and adipose tissue, affects insulin resistance and obesity (34, 35). To avoid indirect effects of whole-organism inactivation of *Pparb/d* on pancreas functions, we generated mice lacking PPARβ/δ specifically in the pancreas. These animals were generated by breeding mice harboring a floxed *Pparb/d* (*Pparb/d*$^{fl/fl}$) (35) to mice expressing the *Cre* transgene under control of the promoter of the gene encoding the transcription factor pancreatic and duodenal homeobox factor 1 (PDX1; Pdx1Cre), in which Cre activity was reported as early as E10.5 (38). In E15.5 Pdx1Cre;R26R mice, Cre expression and subsequent excision of the floxed stop sequence was illustrated by β-gal activity in the PDX1 expression domain, namely the pancreas, caudal stomach, and proximal duodenum (Figure 1D). Deletion of the floxed *Pparb/d* allele was verified by PCR amplification from pancreatic genomic DNA (Figure 1E). The detection of an amplified 490-bp DNA fragment in Pdx1Cre;*Pparb/d*$^{fl/fl}$ (lanes 3 and 4) and Pdx1Cre;*Pparb/d*$^{fl/+}$ (lanes 5 and 6) mice demonstrated the excision of the floxed *Pparb/d* allele (fl). The 2-kb DNA fragment in the absence of the *Cre* transgene (lanes 1 and 2) or presence of the WT *Pparb/d* allele (+) (lane 5–7) demonstrated that the deletion was indeed only present in Pdx1Cre;*Pparb/d*$^{fl/+}$ and Pdx1Cre;*Pparb/d*$^{fl/fl}$ mice, confirmed by the absence of *Pparb/d* mRNA in pancreas and islets isolated from 8-week-old Pdx1Cre;*Pparb/d*$^{fl/fl}$ mice (Figure 1F and Supplemental Figure 1D). Furthermore, nuclear PPARβ/δ was not detected in pancreas and insulin-expressing cells from Pdx1Cre;*Pparb/d*$^{fl/fl}$ embryos (Figure 1G and Supplemental Figure 1E). Elimination of PPARβ/δ did not trigger upregulation of PPARγ and PPARα (Supplemental Figure 1, F and G).

PPARβ/δ deficiency induces hyperinsulinemia and decreased glycemia starting at 4 weeks of age. The Pdx1Cre;*Pparb/d*$^{fl/fl}$ mice were born at the expected Mendelian ratio and showed normal growth and devel-

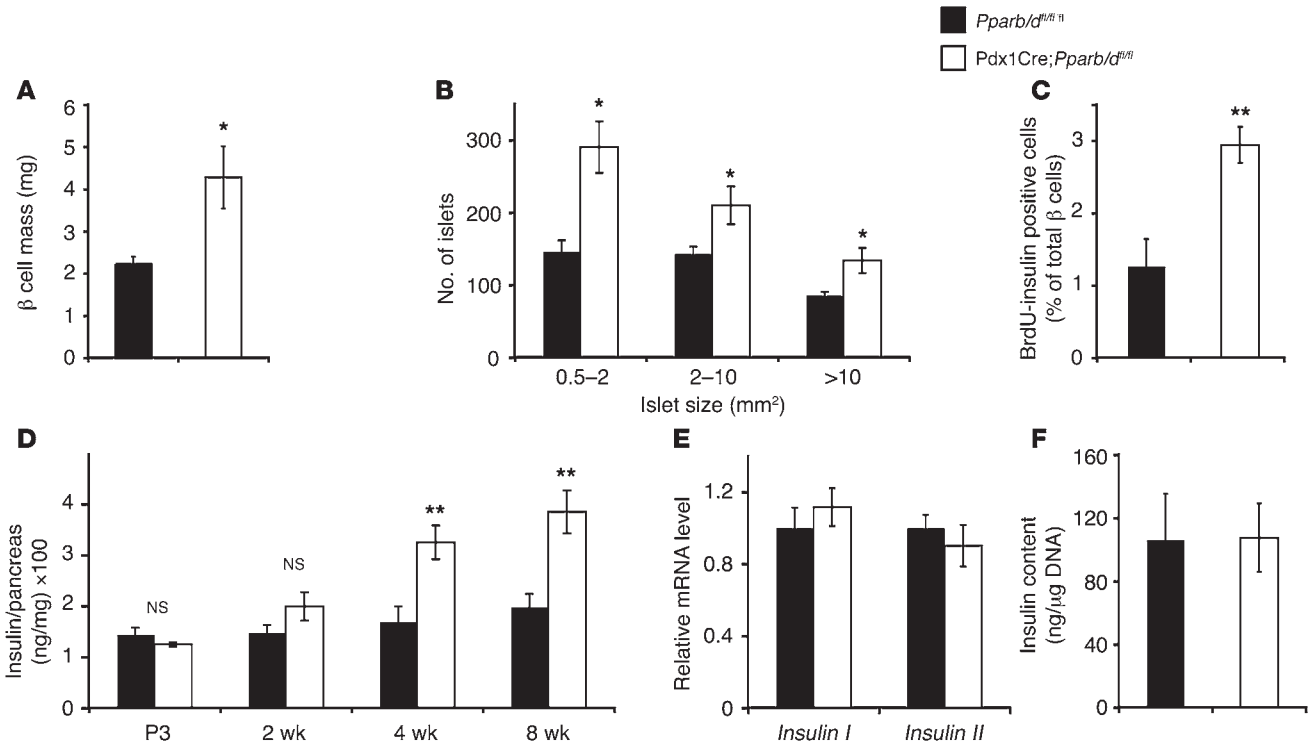

Figure 3
Effect of *Pparb/d* deletion on the pancreas of 8-week-old mice. (**A**) β cell mass quantification ($n = 3$). *$P < 0.05$. (**B**) Islet size distribution derived from pancreas sections used to determine β cell mass ($n = 3$). *$P < 0.05$. (**C**) Quantification of BrdU incorporation in β cells from pancreas section isolated from 2-week-old mice ($n = 4$–5). **$P < 0.01$. (**D**) Pancreatic insulin content at different postnatal stages ($n = 6$). **$P < 0.005$. (**E**) Comparison of *Insulin I* and *Insulin II* mRNA expression levels in islets from 8-week-old mice ($n = 3$). (**F**) Islet insulin content relative to DNA content ($n = 4$).

opment through weaning, as illustrated by body weight at P3 and at weeks 2, 4, 8, and 24 after birth (Figure 2A). In PPARβ/δ mutant mice, plasma insulin levels increased starting at 4 weeks of age, becoming even greater at 8 and 24 weeks when the pancreas is completely mature and functional (Figure 2B). WT 8-week-old mice had plasma insulin levels similar to those of *Pdx1Cre* (0.65 ± 0.12 μg/l vs. 0.76 ± 0.2 μg/l; $P = 0.23$; $n = 7$) and *Pparb/d*$^{fl/fl}$ (0.65 ± 0.12 μg/l vs. 0.86 ± 0.09 μg/l; $P = 0.22$; $n = 10$) mice, indicating that the *Cre* transgene or the loxP element insertions had no effect by themselves on plasma insulin levels. Increased insulin levels in Pdx1Cre;*Pparb/d*$^{fl/fl}$ mice resulted in decreased glycemia, starting at 4 weeks of age, in comparison with that of the *Pparb/d*$^{fl/fl}$ littermates (Figure 2C). When subjected to i.p. glucose tolerance test (GTT), fasted 8-week-old Pdx1Cre;*Pparb/d*$^{fl/fl}$ mice exhibited improved glucose tolerance compared with controls (Figure 2D). Furthermore, their insulin secretion in response to i.p. glucose injection was higher (Figure 2E). However, peripheral glucose assimilation or clearance, assessed by the insulin tolerance test (ITT), was unchanged compared with controls (Figure 2F). Also, plasma α-amylase and glucagon levels did not differ between Pdx1Cre;*Pparb/d*$^{fl/fl}$ (α-amylase = 2731.67 ± 101.6 U/l, $n = 6$; glucagon = 47 ± 5.4 pg/ml, $n = 8$) and *Pparb/d*$^{fl/fl}$ (α-amylase = 2696.43 ± 179.2 U/l, $n = 7$; glucagon = 60.6 ±9.4 pg/ml, $n = 10$) 8-week-old mice, indicating no major defect in pancreatic acinar cells and endocrine α cells, respectively. Taken together, these data demonstrate that a lack of PPARβ/δ in the pancreas led to increased plasma insulin starting at age 4 weeks that caused decreased plasma glucose, while glucose clearance was unchanged.

Precocious inactivation of Pparb/d in the pancreas leads to increased islet numbers. The next question was whether *Pparb/d* excision affects β cell development, which would explain the observed alterations of circulating insulin and glucose levels. Because the *Pdx1* promoter, which controls Cre recombinase expression, becomes active in the foregut epithelium just before the onset of pancreatic bud formation, we assessed alterations in β cell differentiation in the embryonic pancreas. We quantified endocrine precursor neurogenin 3–expressing (Neurog3-expressing) cells and insulin-expressing cells by immunohistochemistry in the E15.5 pancreas. We detected no significant difference between Pdx1Cre;*Pparb/d*$^{fl/fl}$ and *Pparb/d*$^{fl/fl}$ embryonic pancreata and no difference in *Insulin I* and *Neurog3* mRNA levels (Supplemental Figure 2, A–D). Furthermore, there was no alteration in protein level of Neurog3 in pancreas from Pdx1Cre;*Pparb/d*$^{fl/fl}$ compared with *Pparb/d*$^{fl/fl}$ embryos at E17.5 and E18.5 (Supplemental Figure 2E). However, quantitative morphometry demonstrated a 2-fold increase in β cell mass and a 1.5-increase of α cell mass in 8-week-old Pdx1Cre;*Pparb/d*$^{fl/fl}$ mice (Figure 3A and Supplemental Figure 2F) due to increased islet number (Figure 3B and Supplemental Figure 2I). The increase in BrdU incorporation in β cells at 2 weeks of age (Figure 3C) suggested that their higher proliferation at this stage may contribute to the increased islet mass in 8-week-old Pdx1Cre;*Pparb/d*$^{fl/fl}$ mice. At later stages, this difference in islet cell proliferation between PPARβ/δ-deficient and WT animals was not recorded anymore.

To characterize the impact of this β cell mass expansion, we measured pancreas insulin content at P3 and in 2-, 4-, and 8-week-old mice. At P3, PPARβ/δ mutants presented no alteration in total pan-

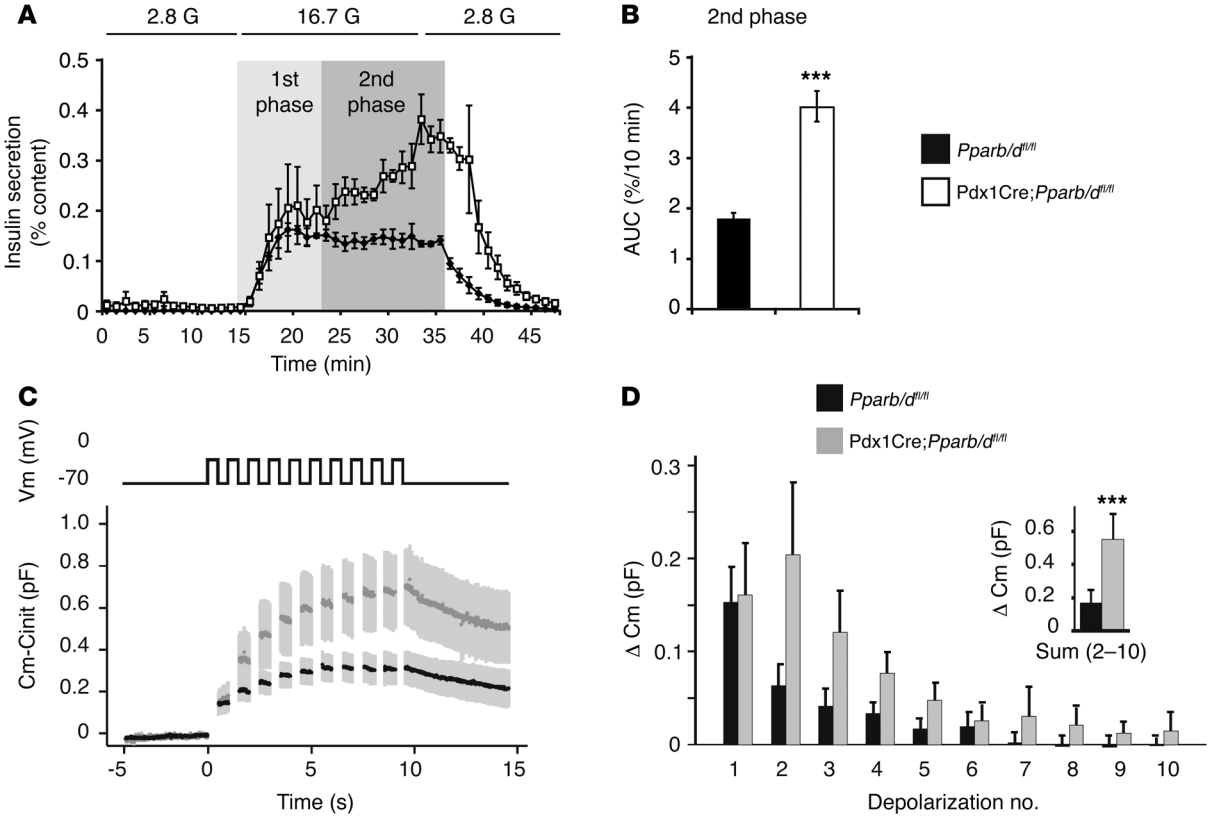

Figure 4

Increased second-phase insulin release in *Pparb/d*-deleted islets. (**A**) Glucose-induced insulin secretion in isolated perifused *Pparb/d*$^{fl/fl}$ (control) and Pdx1Cre;*Pparb/d*$^{fl/fl}$ (KO) islets. Light gray and dark gray zones represent the first and second phases of insulin secretion, respectively ($n = 3$). (**B**) AUC of second-phase GSIS from 25 to 36 minutes on scale. ***$P < 0.005$ ($n = 3$). (**C**) Whole-cell capacitance recordings (Cm) elicited by trains of depolarizations from –70 to 0 mV (top) in isolated control ($n = 15$) and KO ($n = 11$) cells. Averages and SEM (gray) are shown and the initial capacitance (Cinit) was subtracted from the traces. (**D**) Analysis of the relative increase in whole-cell capacitance evoked by each depolarization; inset shows the sum of all the responses during depolarizations 2–10. ***$P < 0.005$.

creatic insulin content (Figure 3D). However, there was a trend toward an increased insulin content in 2-week-old Pdx1Cre;*Pparb/d*$^{fl/fl}$ mice, which became significant at 4 and 8 weeks with a 2-fold increase compared with controls (Figure 3D). There was no difference in insulin mRNA or protein content per β cell in islets isolated from 8-week-old Pdx1Cre;*Pparb/d*$^{fl/fl}$ mice and *Pparb/d*$^{fl/fl}$ control littermates (Figure 3, E and F). Thus, the increase in islet numbers may account for the augmented pancreatic insulin content. Even though in our model, α cells also present the *Pparb/d* deletion, no significant alteration of glucagon content, neither in islets (Supplemental Figure 2G) nor pancreas (Supplemental Figure 2H), was recorded. Collectively, these data showed that *Pparb/d* deletion in pancreas enhanced β cell mass by increasing the number of islets and that the enhanced proliferation of islet cells occurred during the early postnatal period.

Pparb/d deletion in islets enhances second-phase insulin secretion. Because increased β cell number does not always account for hyperinsulinemia and hypoglycemia (39, 40), we tested whether other factors are involved in the phenotype we observed. Thus, we looked into altered β cell functions in Pdx1Cre;*Pparb/d*$^{fl/fl}$ mice, particularly in relation to insulin secretion.

First, we measured GSIS in perifused islets isolated from 8-week-old mice (Figure 4, A and B). At basal levels of glucose (2.8 mM), insulin secretion did not measurably differ between mutated and control islets. In elevated glucose (16.7 mM), islets from Pdx1Cre;*Pparb/d*$^{fl/fl}$ mice exhibited higher insulin release than control islets during second-phase secretion, starting approximately 10 minutes after glucose stimulation. In contrast, insulin secretion during first-phase (first 10 minutes of 16.7 mM glucose induction) was similar in Pdx1Cre;*Pparb/d*$^{fl/fl}$ and control islets (Figure 4A). These data provided evidence that *Pparb/d* deletion in pancreas leads to an enhanced second phase of GSIS, possibly explaining the increased plasma insulin levels in the mutated mice.

Second, we characterized the enhanced insulin secretion of Pdx1Cre;*Pparb/d*$^{fl/fl}$ islets by monitoring exocytosis with whole cell membrane capacitance measurements. During exocytosis, the granular vesicle membrane is incorporated into the plasma membrane, increasing the cell surface. Membrane capacitance is proportional to the cell surface area and is routinely used to measure exocytosis with high temporal resolution in single cells. A single insulin granule will typically contribute to a capacitance increase of approximately 3.5 fF. We noted that initially the mutated cells were larger than controls (8.8 ± 0.4 pF vs. 6.1 ± 0.4 pF, respectively; $P < 10^{-4}$). Exocytosis was elicited by a train (1 s^{-1}) of 10 voltage-clamp depolarizations from –70 to 0 mV, each lasting 500 ms (Figure 4C). The first depolarization triggered a capacitance increase of 153 ± 38 fF in control, not different from the 161 ± 57 fF measured in mutated islets (Figure 4D). How-

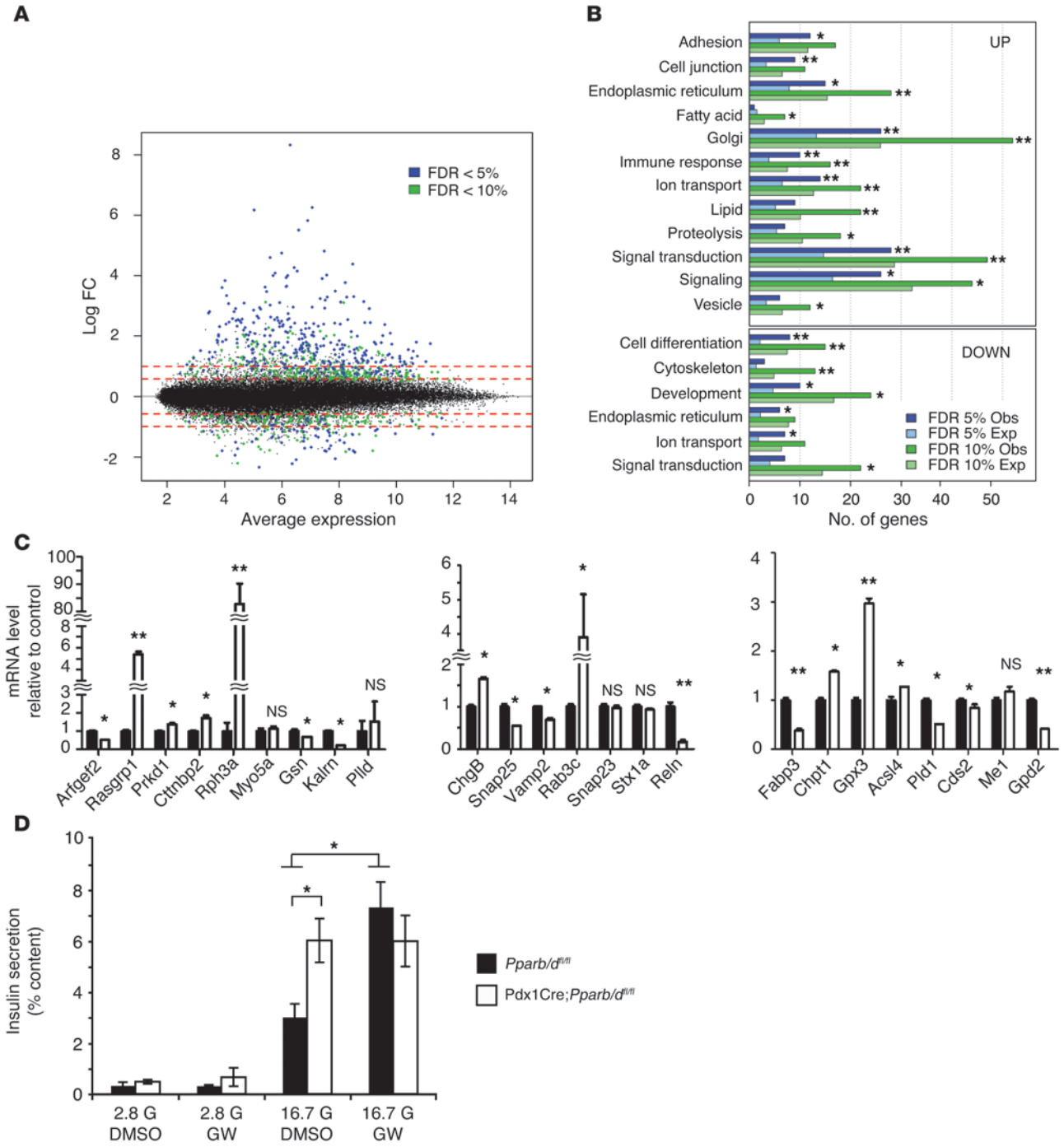

Figure 5

Gene expression profiling in PPARβ/δ-null islets. (**A**) Average expression (log_2) across the 3 *Pparb/d*$^{fl/fl}$ control mice and the 3 Pdx1Cre;*Pparb/d*$^{fl/fl}$ KO mice versus log_2 fold-change between KO and control. Probe sets with a higher expression in KO have a positive fold change. Red dashed lines indicate 1.5-fold and 2-fold changes. Probe sets significantly different at an FDR of less than 5% are indicated in blue and an FDR of more than 5% and less than 10% in green. (**B**) Enrichment of GO annotation terms. Enrichment for annotation terms was performed separately on upregulated and downregulated genes with an FDR of less than 5% or an FDR of less than 10%. Shown are observed (Obs) and expected (Exp) numbers of regulated genes for significant terms. **P* < 0.05; ***P* < 0.01. (**C**) Relative mRNA expression levels in islets from 8-week-old mice determined by qPCR ($n = 3$). **P* < 0.05; ***P* < 0.01. (**D**) Effect of 100 nM of GW501516 (GW) incubation during 24 hours on GSIS from control and KO islets ($n = 3$). **P* < 0.05.

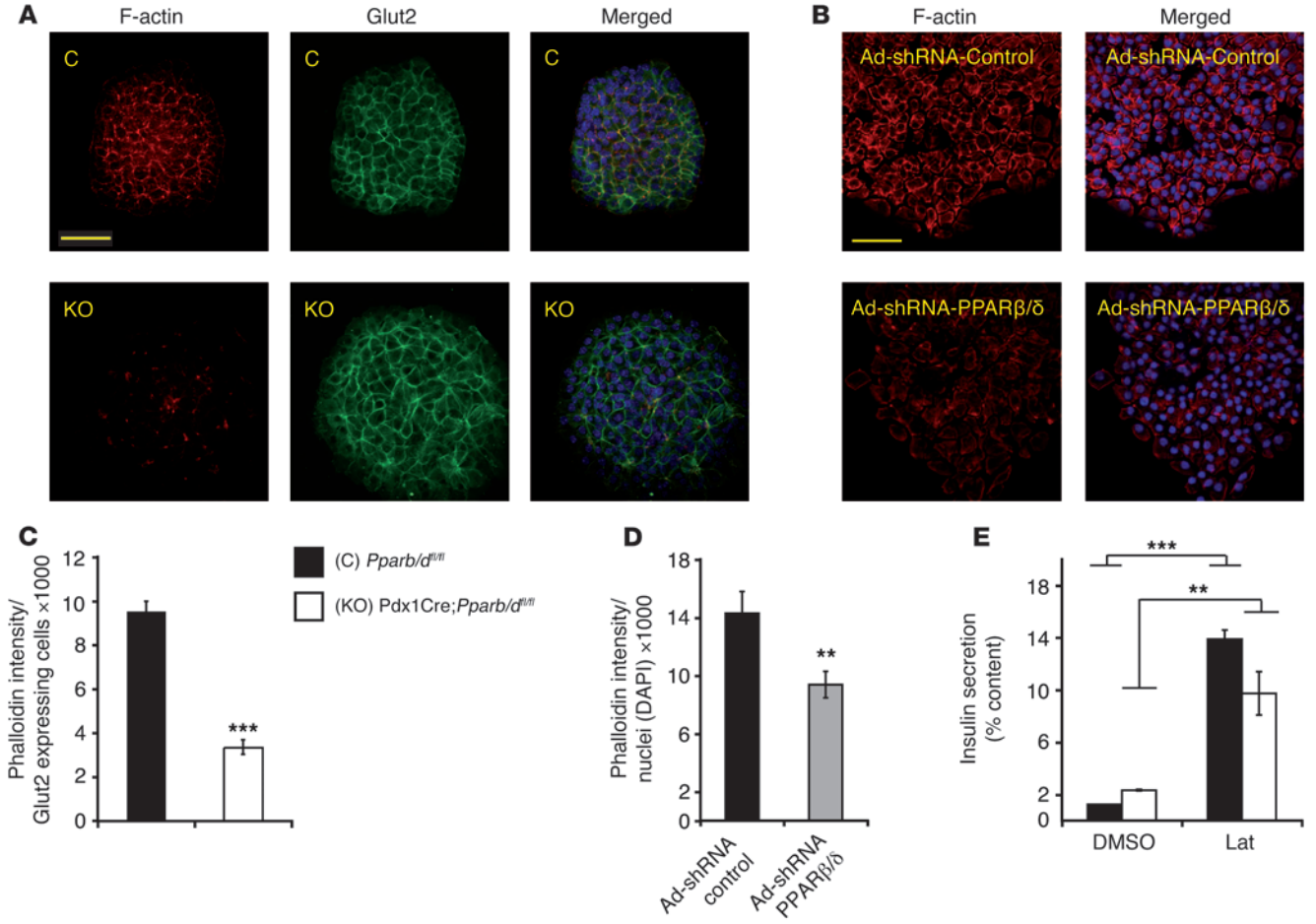

Figure 6

Increased insulin secretion in PPARβ/δ mutant mice is F-actin polymerization dependent. (**A**) Phalloidin (red) and Glut2 (green) staining of islets isolated from *Pparb/d*$^{fl/fl}$ (control) and Pdx1Cre;*Pparb/d*$^{fl/fl}$ (KO) mice. DAPI in blue. Scale bar: 50 μm. (**B**) Phalloidin (red) staining in islets isolated from C57BL/6J mice infected with adenovirus expressing shRNA against PPARβ/δ (Ad-shRNA-PPARβ/δ) and control shRNA (Ad-shRNA-control). Scale bar: 50 μm. DAPI in blue. Quantification of phalloidin fluorescence intensity in control and KO islets (**C**) and in control islets infected with Ad-shRNA-control and Ad-shRNA-PPARβ/δ viruses (**D**). Normalization was according to Glut2-expressing cells and number of nuclei in **C** and **D**, respectively ($n = 3$). $^{**}P < 0.01$; $^{***}P < 10^{-8}$. (**E**) Effect of 10 mM latrunculin (Lat) on GSIS in control and KO islets; ($n = 3$). $^{***}P < 10^{-4}$; $^{**}P < 0.01$.

ever, subsequent depolarizations evoked much larger increases in the mutated cells. The summed response during depolarizations 2 to 10 increased capacitance by 170 ± 77 fF in controls, less than a third of the 551 ± 144 fF in mutated cells (Figure 4D, $n = 15$ vs. 11, $P < 10^{-4}$). The increase in evoked exocytosis is unlikely to be due to accelerated influx through voltage-gated Ca^{2+} channels because the charge and peaks of the associated Ca^{2+} currents were similar in both groups (18.3 ± 2.3 pC vs. 20.2 ± 4.2 pC and 118 ± 18 pA vs. 112 ± 16 pA in mutated and control cells, respectively). This was further confirmed by measurements of cytosolic Ca^{2+}, revealing no differences between mutated and control cells and indicating that Ca^{2+} handling played no role in the mutated islet phenotype. Glucose-induced (7.5 ± 2.7 vs. 10.4 ± 3.6, $P = 0.1$) or KCl-induced (9.2 ± 2.9 vs. 10.4 ± 2.0, NS) opening of voltage-dependent Ca^{2+} channels and resulting changes in cytosolic free Ca^{2+} concentration also did not differ between mutated and control islets (Supplemental Figure 3, A–C).

Third, we quantified membrane-docked granules using total internal reflection fluorescence (TIRF) microscopy in islets expressing the dense-core granule marker NPY-venus. TIRF allows the observation of single fluorescence-tagged vesicles at the cell membrane that undergo exocytosis and release their fluorescent cargo. The density of granules near the β cell plasma membrane did not differ between unstimulated mutated and control islets (0.99 ± 0.08 g/μm^2; $n = 24$ cells vs. 0.92 ± 0.05 g/μm^2; $n = 56$ cells, not shown), in agreement with a similar first-phase insulin secretion in both genotypes.

To analyze whether the mixed background of the experimental mice might be responsible for the increased insulin secretion observed in Pdx1Cre;*Pparb/d*$^{fl/fl}$ islets, we assessed GSIS in islets isolated from C57BL/6J mice, which were infected with adenovirus expressing shRNA against PPARβ/δ, which reduced *Pparb/d* mRNA expression by 70% (Supplemental Figure 3D). These PPARβ/δ-deficient islets presented a 2.5-fold increase of 16.7 mM GSIS compared with control islets (Supplemental Figure 3D). It is noteworthy that there was PPARβ/δ knockdown–induced insulin secretion already at 2.8 mM glucose, which was strongly increased at 16.7 mM glucose (Supplemental Figure 3D). On the contrary, reexpression of PPARβ/δ in PPARβ/δ-deficient

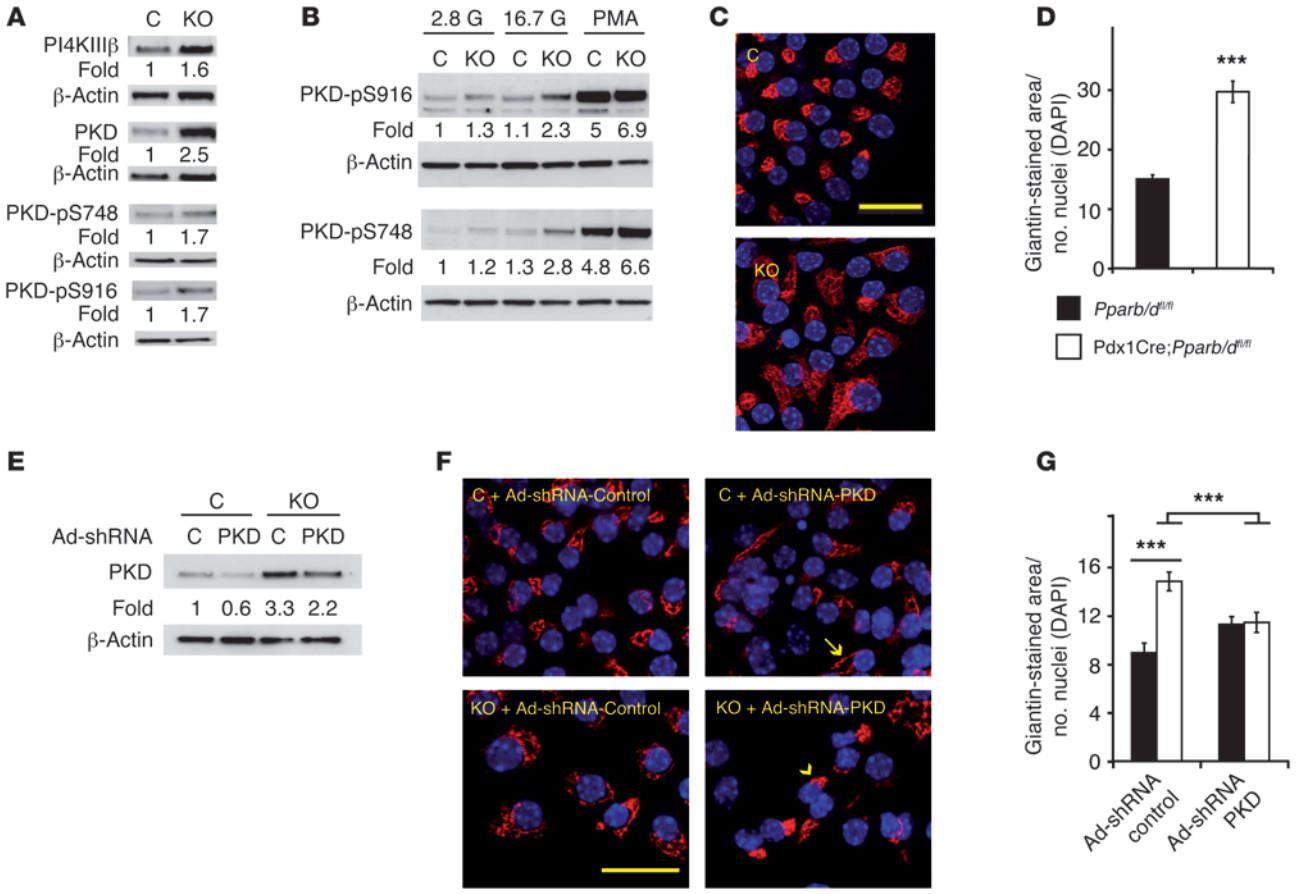

Figure 7
Altered Golgi organization in PPARβ/δ-deficient islets. (**A**) PI4KIIIβ, PKD1 protein, pS748-PKD1, and pS916-PKD1 levels in islets isolated from *Pparb/d*$^{fl/fl}$ (control, C) and Pdx1Cre;*Pparb/d*$^{fl/fl}$ (KO) mice. (**B**) Effect of 2.8 and 16.7 mM of glucose and 300 nM of PMA on PKD1 phosphorylation at serines 916 and 748 in islets from control and KO mice. (**C**) Representative pictures of immunostaining of giantin (red) in control and KO islets. Scale bar: 20 μm. (**D**) Quantification of giantin-stained areas normalized by the number of nuclei (DAPI) (n = 10–15 islets from 3 mice). ***$P < 10^{-4}$. (**E**) PKD1 protein levels in control and KO islets infected with adenovirus expressing shRNA against PKD1 (Ad-shRNA-PKD1) and control shRNA (Ad-shRNA-control). (**F**) Representative photographs of control and KO islets infected with Ad-shRNA-control and Ad-shRNA-PKD1 adenovirus. Yellow arrow shows the tubular protrusions in Golgi apparatus. Yellow arrowhead shows normal nucleus-adjacent Golgi apparatus. Scale bar: 20 μm. (**G**) Quantification of giantin stained areas normalized by the number of nuclei (DAPI) in control (C) and KO islets infected with Ad-shRNA-control and Ad-shRNA-PKD viruses (n = 10–15 islets from 3 mice). ***$P < 10^{-4}$.

Pdx1Cre;*Pparb/d*$^{fl/fl}$ islets via an adenovirus expression vector decreased insulin secretion in islets incubated at 16.7 mM glucose (Supplemental Figure 3E).

Collectively, these data demonstrate that *Pparb/d* deletion in the pancreas accelerated granule exocytosis and second-phase insulin secretion, while the initial size of the RRP remained unaffected. Importantly, these effects were independent of the mouse strains.

Global gene expression profile of PPARβ/δ-deficient islets. To examine the possible causes of disturbance in the complex second-phase insulin secretion, we used Affymetrix microarrays to compare mRNA expression profiles of islets isolated from 8-week-old Pdx1Cre;*Pparb/d*$^{fl/fl}$ with *Pparb/d*$^{fl/fl}$ mice as controls. First, we found many more genes positively rather than negatively affected in Pdx1Cre;*Pparb/d*$^{fl/fl}$ islets, indicating a broad gene inhibitory action of PPARβ/δ in these cells.

At a false discovery rate (FDR) threshold of 5%, 321 probe sets had significantly increased expression and only 83 probe sets showed significantly decreased expression in Pdx1Cre;*Pparb/d*$^{fl/fl}$ mice (Figure 5A). At an FDR threshold of 10%, the numbers were 606 and 269 for the probe sets with increased and decreased expression, respectively. To identify cellular functions affected in the null cells, we devised an annotation term enrichment strategy based on the Gene Ontology (GO) annotation (Figure 5B). Briefly, we counted the number of occurrences of the different GO terms in the list of up- or downregulated genes. Then, we chose functionally informative words to represent part or all of the most abundant GO terms. These words were then tested for overrepresentation among regulated genes (Supplemental Table 2). Considering the role of PPARs in attenuating the inflammatory response, it was perhaps not surprising that genes related to the immune response were upregulated in the null cells (41, 42). The terms *lipid* and *fatty acid* were prevalent among upregulated genes with FDRs of less than 10%, but not among genes with FDRs of less than 5%. On the other hand, the term *ion transport* was highly prevalent among genes with FDRs of less than 5%, both up- and downregulated. The terms *adhesion* and *cell junction* were enriched among upregulated genes,

and the term *cytoskeleton* was enriched among downregulated genes. These findings may reflect a role of PPARβ/δ in cell chemotaxis, polarization, and migration, as observed in keratinocytes (27). Finally, genes related with *vesicles* and the *Golgi system* were enriched among upregulated genes in Pdx1Cre;*Pparb/d*$^{fl/fl}$ islets, in agreement with enhanced insulin secretion by the mutated islets.

In order to validate the cytoskeleton and fatty acid gene expression profiles, quantitative PCR (qPCR) was performed on RNA samples from islets isolated from 8-week-old mice (Figure 5C). As observed in the microarray analysis, PPARβ/δ-deficient islets presented alterations in the expression of genes coding for the guanine nucleotide exchange factor–activated (GEF-activated) small GTPases implicated in the regulation of the cytoskeleton (*Arfgef2*, *Rasgrp1*, and *Kalrn*), the actin-polymerization regulators (*Gsn* and *Reln*), and the granule-trafficking regulators (*Rph3a* and *Rab3c*). Also interestingly, markers for secretion (*ChgB*) and oxidative stress (*Gpx3* and *Me1*) were increased in *Pparb/d*-null islets. Similarly, fatty acid regulators in the Golgi membrane (*Chpt1*, *Pld1*, and *Prkd1*) also had an altered expression in PPARβ/δ-deficient islets.

We speculated that apo-PPARβ/δ mediates the unveiled broad repression activity on insulin secretion, which is similar to its inhibitory activity in early development during gastrulation (Nicolas Rotman and Walter Wahli, unpublished observations). In support of this hypothesis, treatment of islets with a PPARβ/δ ligand during GSIS increased secretion to levels observed in *Pparb/d*-null islets (Figure 5D), which is consistent with an agonist-dependent alleviation of repression. The molecular mechanism of this effect remains to be investigated.

Based on the gene expression results and the interesting observations in insulin secretion, we then concentrated our study on the β cell insulin secretion pathway.

PPARβ/δ has an impact on the insulin secretory pathway at multiple sites. The enhanced second phase of secretion in the absence of PPARβ/δ suggests a higher flux of secretory granules to the plasma membrane for insulin release, which might be caused by an increased rate of granule fission at the trans-Golgi network (TGN), an unimpeded transport of insulin granules through the cortical actin meshwork, and a more efficient insulin exocytosis at the plasma membrane.

In fact, the gene expression–profiling data presented above provided support for important deregulations of genes with functions in granule biosynthesis, vesicle trafficking, and exocytosis. For instance, the most deregulated gene after *Pparb/d* deletion encodes rabphilin (*Rph3a*) (Figure 5C), a Rab 3-GTP binding protein concentrated on secretory vesicles of neurons and endocrine cells (43). Similarly, *Rab3C*, also encoding a GTP-binding protein that colocalizes with secretory vesicles and plays a role in exocytosis (44), was upregulated. Furthermore, enhanced expression of the RAS guanyl releasing protein 1 (*Rasgrp1*) gene, which mediates the effects of acetylcholine through calcium and DAG binding, may also increase insulin secretion (45).

Polymerized cortical actin is known to form a barrier for insulin granule movement toward the plasma membrane, thereby limiting exocytosis (46, 47). Because GO analysis revealed that the expression of several cytoskeleton-related genes was decreased (Figure 5B), we analyzed the distribution of F-actin in β cells lacking PPARβ/δ. Quantification of the F-actin by phalloidin immunostaining on ECM-plated islets showed a 3-fold decrease in F-actin intensity in Pdx1Cre;*Pparb/d*$^{fl/fl}$ islets compared with control islets (Figure 6, A and C). In addition, 80% knockdown of *Pparb/d* mRNA levels in C57BL/6J islets (Supplemental Figure 3D) reduced F-actin polymerization by 40% (Figure 6, B and D). Pdx1Cre;*Pparb/d*$^{fl/fl}$ and control islets did not differ in β-actin protein level (Figure 7A) or in globular actin staining (Supplemental Figure 4), suggesting a decrease of polymerized actin in mutated β cells, identified in this experiment as Glut2-expressing cells (Figure 6A), rather than a diminution of the total amount of actin.

It was proposed previously that glucose causes a transient reduction of cortical filamentous actin (F-actin) to promote granule mobilization and pool refilling, which ultimately increases granule exocytosis (48). To determine whether reduced F-actin in PPARβ/δ mutant islets promotes insulin secretion, we experimentally broke the cortical F-actin barrier. We assessed the effect of latrunculin, an F-actin–depolymerizing drug, on GSIS. Latrunculin increased 16.7 mM GSIS 11-fold in control islets, but only 4-fold in Pdx1Cre;*Pparb/d*$^{fl/fl}$ islets (Figure 6E). This result is compatible with a higher level of F-actin and thus a stronger effect of latrunculin in PPARβ/δ WT compared with Pdx1Cre;*Pparb/d*$^{fl/fl}$ islets. Taken together, these data implicate PPARβ/δ in an F-actin filament network that decreases GSIS in WT pancreatic β cells. We conclude that reduced actin filament polymerization in mutated cells is likely to increase second-phase insulin secretion.

Finally, the transcriptomic analysis indicated upregulation of several Golgi genes (Figure 5B), including *Prkd1*. Recent work revealed a key role of the Golgi-associated kinase PKD1 (also called PKCμ) in TGN structure maintenance, export granule fission, and insulin secretion (17). Furthermore, PKD1 effects are mediated, at least in part, by phosphorylation of PI4KIIIβ (49, 50). These results prompted us to assess the impact of *Pparb/d* deletion on the Golgi apparatus. We measured the protein level of PI4KIIIβ as well as the level and phosphorylated state of PKD1 in islets isolated from 8-week-old mice. Compared with control islets, PPARβ/δ-deficient islets expressed 2.5- and 1.6-fold more PKD1 and PI4KIIIβ, respectively (Figure 7A). Furthermore, phosphorylation of PKD1 at the catalytic (serine-748) and autophosphorylation (serine-916) residues, known to result in a higher PKD1 activity, was increased not only in non–glucose-stimulated *Pparb/d*-null islets (Figure 7A), but also in 30-minute glucose-stimulated islets (Figure 7B). As overactivation of PKD1 alters Golgi membrane structure (17), we monitored the localization of the Golgi marker giantin and the TGN marker TGN38 by immunofluorescence microscopy in isolated β cells. In the absence of PPARβ/δ, both markers showed an extended and more diffused distribution compared with the expected compact nuclear proximal structures in the WT cells (Figure 7, C and D, and Supplemental Figure 5A). Expanded giantin distribution was not due to increased levels of the protein (Supplemental Figure 5D). To determine whether the PKD1 signaling pathway was indeed involved in this Golgi membrane alteration, *Pparb/d*-null and control islets were infected with adenovirus expressing shRNA against *Prkd1*. A decrease of the PKD1 level (Figure 7E) reversed the giantin distribution observed in PPARβ/δ-deficient β cells (Figure 7, F and G), while in control islets, it generated tubular protrusions on the Golgi apparatus, as reported previously (Figure 7F) (17). In addition, treatment with a PKD1 inhibitor (Gö6976) reversed giantin distribution in PPARβ/δ-deficient β cells, which became similar to that in control islets (Supplemental Figure 5, B and C). These observations suggest that PPARβ/δ participates in mechanisms regulating membrane fission at the TGN through the regulation of PKD1 activity.

Collectively, the data gained from the analysis of the impact of PPARβ/δ on the insulin secretion pathway revealed what we believe are novel functions of this receptor. PPARβ/δ, most likely in its apo

form, plays an essential role in limiting β cell secretion by acting in a coordinated manner on at least 3 different steps of GSIS: the production of insulin granules from the TGN, the control of cortical actin as a barrier for granules toward the plasma membrane, and the production of regulators of insulin granule exocytosis.

Discussion

This study identifies a previously unrecognized role of PPARβ/δ in insulin secretion associated with a broad repressive effect on islet β cell gene expression. Removal of this inhibitory action by deletion of *Pparb/d* in pancreas led to a higher number of islets and enhanced insulin release during the second phase of GSIS. We propose that the unexpected consequent morphological disturbances of the β cell, namely actin cytoskeleton disorganization and altered Golgi apparatus, participated in this enhanced insulin release. Changes in the plasma levels of insulin and glucose in mice with *Pparb/d*-null pancreatic cells became apparent after weaning, when the pancreas normally reaches its adult size and has acquired its definitive morphology and functions.

Several observations reported herein support the notion that the enhanced insulin secretion reported in these mutant mice is due to the deletion of the *Pparb/d* gene in β cells rather than in non-β cells, even though similar expression levels of PPARβ/δ in α and β cells were noted in WT mice. Thus, increased GSIS and cytoskeleton disorganization in cultured C57BL/6J islets in which PPARβ/δ was knocked down make a role of acini in the PPARβ/δ-controlled regulation of these processes unlikely. Furthermore, capacitance measurements performed in single cells from dissociated islets, which were electrophysiologically identified as β cells, revealed enhanced exocytosis in PPARβ/δ-deficient β cells, excluding a direct role of α cells in the accelerated exocytosis.

PPARβ/δ regulates pancreatic β cell mass in neonatal stages. Pancreatic deletion of *Pparb/d* did not alter the development of islets at the embryonic, but at the neonatal stage. Pancreatic insulin content and RNA expression of endocrine markers (Supplemental Table 1) were normal in PPARβ/δ-deficient pancreas at P3. In contrast, these mice presented an increase of RNA expression of endocrine markers and β cell proliferation at P14, suggesting an important role of PPARβ/δ in β cell mass regulation in neonatal stages, which correlates with the enhanced expression of this nuclear receptor in pancreas at P14. Interestingly, at 8 weeks of age, the β cell mass remained higher in the mutated pancreata, but β cell proliferation returned to normal. Hence, *Pparb/d* deletion in pancreas may alter the neonatal remodeling of β cell mass, which normally occurs from P9 to P31 in rat (51). This remodeling period is likely to account for the enhanced β cell mass at 8 weeks of age in the mutated mice. Decreased *p27Kip1* mRNA expression in PPARβ/δ-deficient islets (fold change –1.5; $P < 0.003$) may underlay the accelerated proliferation at neonatal stages in the mutant mice. Interestingly, overexpression of p27Kip1 reduces pancreatic β cell proliferation only when applied during neonatal and postnatal development (52), suggesting a special gene expression program regulating postnatal β cell mass. How PPARβ/δ is implicated in this program remains to be determined.

The absence of PPARβ/δ affects second-phase insulin release. Altered β cell mass does not necessarily correlate with disturbances in plasma insulin levels (40). Hence, we hypothesized that insulin secretion changes may contribute to the hyperinsulinemia in 8-week-old PPARβ/δ-deficient mice. We found both enhanced second-phase insulin secretion from perifused islets and an increased rate of sustained exocytosis in *Pparb/d*-null β cells as assessed by capacitance measurements. Changes in Ca^{2+} handling do not explain enhanced GSIS in *Pparb/d*-null islets because evoked Ca^{2+} currents and measured intracellular [Ca^{2+}] were similar in PPARβ/δ mutant and control islets. Also, TIRF microscopy analysis showed similar numbers of docked granules in control and PPARβ/δ-deficient islets, indicating that the formation of the RRP of granules proceeds normally. In contrast, this suggested an increased efficiency of recruitment and exocytosis of secretory granules coming from internal stores and/or newly formed at the TGN. Indeed, microarray analysis provided support for multiple other mechanisms augmenting insulin secretion in the mutated islets.

First, the exocytotic step may be increased because of the dramatically higher expression of rabphilin 3a (Figure 5C), as has been shown in β cells with forced overexpression of this protein (43, 53). There was also a 1.4-fold decrease of neurexin 1α ($P < 0.004$) in PPARβ/δ-deficient islets. This protein functionally interacts with granuphilin in the docking of secretory granules. In addition, mice null for neurexin 1α present an increased second-phase insulin secretion (54).

Second, second-phase insulin secretion requires mobilization of RP granules during prolonged glucose stimulation. These granules must cross the F-actin network beneath the cell surface to reach their release site at the cell membrane. Granule mobilization for RRP refilling is tightly associated with F-actin remodeling, which involves actin filament disassembly (55). Here, we observed actin cytoskeleton disorganization in *Pparb/d*-null islets with reduced basal amounts of F-actin in the absence of glucose stimulation. This drastic alteration in the F-actin network already at basal levels (before glucose stimulation) suggests that other factors to be identified have a dominant impact on F-actin in *Pparb/d*-null β cells. We propose that this defect in cytoskeleton disorganization facilitates second-phase insulin secretion. In agreement with this conclusion, we have shown that an actin depolymerization agent (latrunculin) potentiates GSIS in WT islet much more than in PPARβ/δ-deficient islets, which is consistent with strongly reduced F-actin in the latter.

Third, *Pparb/d*-null β cells also display an alteration of the Golgi network, and our study showed that this was caused by an overactivation of the Golgi-associated PKD1. PKD1 regulates membrane fission at the TGN, promoting formation of transport vesicles and priming them for efficient routing to the cell membrane (56). PI4KIIIβ is an essential target of PKD1 action in this vesicular traffic (50). *Pparb/d*-null β cells show an increase in expression of both proteins and phosphorylation of PKD1. This could account for part of the augmented secretory activity of these islets, as shown in mice lacking the MAPK *p38*δ, which exhibit an increased insulin secretion phenotype similar to that described here (17). This defect was demonstrated to result from lack of phosphorylation of PKD1 on inhibitory serine residues, leading to overactivity of this kinase, deregulated Golgi structure, and increased insulin secretion. Also, DAG is required for activation of PKD1 to promote vesicular fission from TGN (49). Enzymes implicated in the accumulation of DAG on TGN, as sphingomyelin synthase 1 and DAG cholinephosphotransferase 1, showed 1.5-fold ($P < 0.001$), and 2.2-fold ($P < 10^{-6}$) increases of their mRNA in PPARβ/δ-deficient islets, respectively. Therefore, we propose that increased PKD1 levels and activity in mice lacking PPARβ/δ affect the Golgi/TGN without influencing insulin production, which is in agreement with unmodified insulin content in the mutated β cells.

Conclusion. Our work revealed what we believe are novel and thus-far-unrecognized roles for PPARβ/δ in pancreatic β cell functions. We used a pancreas-specific deletion of *Pparb/d* to confirm that the changes we observed are not attributable to indirect effects that would arise from a whole-organism *Pparb/d* deletion. A first insight into PPARβ/δ functions came from gene expression profiling, which unveiled an unexpectedly broad gene expression–repressive function of this receptor isotype in β cells, most likely in its apo form. The second insight was that the systemic impact of depleting pancreatic PPARβ/δ, i.e., hyperinsulinemia and lower glycemia, results from alterations in basic cellular functions, such as Golgi functions and actin cytoskeleton-dependent routing of granules to the cell periphery. In fact, this study identified PPARβ/δ as a master regulator of functions associated with each step of insulin secretion, i.e., granule biosynthesis, vesicle trafficking, and exocytosis. Targeting PPARβ/δ with tissue-specific modulators might offer a novel approach to stimulating β cell survival and insulin release under conditions of sustained glucose stimulation as encountered in type 2 diabetes.

Methods

Mouse models. *Pparb/d*$^{fl/fl}$ mice (35) having exon 4 (which encodes the N-terminal zinc finger of the DNA-binding domain) of the *Pparb/d* gene flanked by loxP sites were mated with mice carrying the *Cre* transgene under the control of the Pdx1 promoter, which we refer to as Pdx1Cre (38). The Pdx1Cre^{+};*Pparb/d*$^{fl/+}$ progeny males were bred with *Pparb/d*$^{fl/fl}$ females to obtain Pdx1Cre^{+};*Pparb/d*$^{fl/fl}$ mice. To maintain this genotype, we mated the Pdx1Cre;*Pparb/d*$^{fl/fl}$ males with *Pparb/d*$^{fl/fl}$ females. Some *Pparb/d*$^{fl/fl}$ mice were bred with Pdx1Cre/R26R to obtain Pdx1Cre;*Pparb/d*$^{fl/fl}$;R26R. Pdx1Cre^{+} mice were mated with Pdx1Cre^{-} mice (WT mice) to maintain the Pdx1Cre and WT control mice. The Pdx1Cre and R26R transgenes (57) were maintained in hemizygote conditions. All the mice were bred on a mixed genetic background (SV 129/C57BL/6). All the animals were housed in our SPF facility on a 12-hour light/12-hour dark cycle and were fed with a standard laboratory chow diet.

Metabolic studies and endocrine hormone content in pancreas and islets. Blood collection from the tail vein was performed in fed mice between 8:00 and 10:00 am. Blood collection from P3 mice was carried out by decapitation. Insulin determination was performed with 10 μl of plasma or 10 μl of 1/5,000 pancreatic acid–ethanol extracts by using an ultrasensitive mouse insulin ELISA. For glucagon determination, we used 50 μl of plasma or 50 μl of 1/1,000 pancreatic acid–ethanol extracts by using RIA (Linco). Glycemia was measured with the Accu-Chek Aviva System (Roche Diagnostics). The GTT was performed in animals fasted for 12 hours by i.p. injection of glucose (2 mg/g), and at the indicated time, the glycemia was assessed from tail blood samples. For the insulin secretion experiments, mice fasted 12 hours were i.p. injected with glucose (3 mg/g), as described for GTT experiments. Regarding ITT, chow-diet–fed animals were i.p. injected with insulin (0.75 U/g), and glucose determination was done at the indicated time. Insulin and glucagon content were determined from 30 sonicated islets in lysis buffer (TRIS buffer, pH 7.5, and 1% Triton X-100) by ELISA (Mercodia) and RIA (Linco), respectively. In islets, insulin content was normalized by DNA quantification with Hoechst, whereas glucagon content was normalized by total protein amount with BCA.

Immunohistochemistry in pancreas and islets. Pancreata from embryos (E15.5 and E17.5) or adult mice (2 and 8 weeks of age) and ECM-plated islets were washed with PBS and fixed immediately in 4% paraformaldehyde at 4°C overnight and 10 minutes, respectively. X-gal staining and immunohistochemistry procedures are described in Supplemental Methods. The primary antibodies were used at the following dilutions: guinea pig anti-swine insulin (Dako), 1/400; rat anti–e-cadherin (Abcam), 1/1600; rabbit anti-Glut2 (gift of Bernard Thorens, Center for Integrative Genomics, University of Lausanne, Switzerland), 1/1000; rabbit anti-giantin (Covance Inc.), 1/1,000; sheep anti-TGN38 (AbD Serotec), 1/500; rabbit anti-Neurog3 (Santa Cruz Biotechnology Inc.), 1/1,000; and rabbit anti-PPARβ/δ (Thermo Scientific, Inc.), 1/200.

Determination of β cell mass and proliferation. Pancreata from 3 Pdx1Cre;*Pparb/d*$^{fl/fl}$ and 3 *Pparb/d*$^{fl/fl}$ 8-week-old mice were processed to determine the islet β cell mass by using the following equation: β cell mass = pancreas weight (mg) × relative insulin surface (total islet area μm^2 /total pancreas area μm^2) × 100. For details see Supplemental Methods. Pancreata from 2- and 8-week-old mice, previously injected with BrdU, were sectioned and stained against anti-BrdU (Roche Applied Science) and anti-insulin. The sections were analyzed by confocal microscopy (Zeiss) and BrdU/insulin-expressing cells were counted with ImageJ.

Fluorescence quantification. For staining of F- and G-actin, giantin, Glut2, and TGN38, we plated 10–15 islets for mice (n = 3) on ECM (Novamed) in RPMI medium for 2 days in the case of KO mice or 3 days for adenovirus-infected islets. For F-actin and G-actin determination, we performed phalloidin-rhodamine (Invitrogen), and DNAse I Alexa Fluor 488 conjugate (Invitrogen) staining, respectively. Giantin staining was performed in adenovirus-infected or noninfected islets that were incubated with or without 1 μM of Gö6976 (Calbiochem) for 12 hours in RPMI 1640 medium supplemented with 5 mM of glucose. Stained islets were imaged by confocal microscopy (Zeiss); phalloidin fluorescence intensity and giantin-stained area were quantified by ImageJ software and normalized by Glut2-expressing cells and DAPI-stained nuclei, respectively.

Pancreatic islets isolation and glucose insulin-stimulated secretion. Islet isolation was accomplished from 8-week-old mice by 100 mg of collagenase digestion (211 U/mg) followed by purification through a Histopaque gradient. Islet perifusion was carried out by placing 30 islets into a perifusion chamber (Millipore) as described previously (58). To increase the glucose secretion, we supplemented the Krebs-Ringer bicarbonate buffer (KRBH) with 50 μM of 3-isobutyl-1-methylxanthine (IBMX). We determined the insulin concentration by RIA from each fraction collected. The insulin secretion was normalized with the insulin content that remained in the islets after perifusion. GSIS was performed by preincubating 10 adenovirus-infected or noninfected islets in KRBH, pH 7.4, supplemented with 2.8 mM of glucose, with or without 10 mM latrunculin (Calbiochem) for 1 hour at 37°C, in triplicate for each mouse (set of 10 islets). Then, we incubated the islets in KRBH with 2.8 or 16.7 mM of glucose, with or without latrunculin, for 1 hour at 37°C. For PPARβ/δ agonist treatment, the islets were starved for 16 hours in RPMI without FBS before incubation with or without 100 nM of GW501516 for 24 hours at 37°C. Then the islets were incubated in glucose as above. Finally, we determined the insulin secreted in the buffer by using an ultrasensitive mouse insulin ELISA; the insulin secretion was normalized by total insulin content from islets (acid-ethanol preparation).

Adenovirus infection of pancreatic islets. Islets were isolated as previously described and infected with recombinant adenoviruses at a multiplicity of infection of 200, 48 hours before utilization. After isolation, islets were gently dissociated using HBSS containing 5 mM glucose 1 mM EGTA at 37°C for 3 minutes before being put in contact with recombinant adenoviruses: 200 islets per well in a 12-well plate (nunc NC-150200) for 3 hours at 37°C. To overexpress PPARβ/δ, we used recombinant adenoviruses expressing GFP alone or human PPARβ/δ-GFP (Vector Lab), both under CMV promoter control. To knock down *Pparb/d* and *Prdk1*, we used recombinant adenoviruses coexpressing GFP with an shRNALuc as control or shRNA mouse sequences 5′-CACATCTACAACGCCTAC-3′ and 5′-CAGGAAGAGATGTAGCTAT-3′ against *Pparb/d* and *Prdk1*, respectively.

RNA preparation from pancreatic α and β cells sorted by FACS. Pancreata were injected with 5 ml collagenase V (0.5 mg/ml) in Ca^{2+}- and Mg^{2+}-free HBSS, dissected from the surrounding tissue, and transported on ice. Following an 11-minute digestion at 37°C, the pancreas was disrupted by vigorous shaking, and the islets were transferred by manual picking into HBSS containing 10 mM glucose and 0.1% BSA. Islets were disrupted by trituration in 0.1× trypsin/EDTA, and 10% FCS was then added. Cells were separated immediately using a MoFlo Beckman Coulter Cytomation Sorter (488 nm excitation). Single cells were selected by their forward scatter and pulse width, α cells were selected on the basis of their relative Venus fluorescence at 530 and 580 nm, and β cells were selected by their high side scatter, absence of Venus fluorescence, and high background autofluorescence at 530 nm (59). From 10,000 to 30,000 cells were collected into lysis buffer (Ambion), and the total was isolated using a microscale RNA isolation kit (Ambion).

Capacitance and intracellular Ca^{2+} measurements. Measurements of exocytosis were performed in the whole cell configuration using an EPC-9 amplifier controlled by Pulse software (both HEKA Elektronik). Intracellular Ca^{2+} measurement was performed by fluorescence in islets incubated with FURA-RED AM (Invitrogen). For details, see the Supplemental Methods.

TaqMan qRT-PCR and microarray. Total RNA from islets or pancreata was extracted using guanidine thiocyanate (Sigma-Aldrich). For qRT-PCR, we used TaqMan probes (Applied Biosystems) and primers for SYBR-green detection. cDNA from human islets was obtained from M. Prentki's laboratory (Montreal Diabetes Research Center and CRCHUM, and the Departments of Nutrition and Biochemistry, University of Montreal). For microarray analysis, we amplified 5 ng of total islet RNA (from each mouse) and labeled it using the GeneChip IVT labeling kit according to the protocol provided by the supplier. For details, see Supplemental Methods. Microarray data have been deposited (GEO GSE16048).

Western blot analysis. Approximately 300 islets were lysed in lysis buffer supplemented with protease (Roche) and phosphatase (Sigma-Aldrich) inhibitors. A total of 10–20 μg of total protein extracts were resolved by SDS–10% polyacrylamide gels and electrotransferred onto a nitrocellulose membrane (Whatman). We developed the membrane using a chemiluminescence ECL system (Amersham), with anti-PI4KIIIβ (Millipore), anti–PKD1-pSer 748 (Abcam), anti-Neurog3 (Santa Cruz Biotechnology Inc.), anti-giantin (Covance Inc.), anti-PKD1, anti–PKD1-pSer 916, and anti–β-actin from Cell Signaling Technology. To assess the effect of glucose and PMA on PKD1 phosphorylation, we processed the islets in the same way as in the GSIS experiment, but the incubation was for 30 minutes at 2.8 or 16.7 mM of glucose or 300 nM of PMA as positive control. 20 μg of total protein extracts were resolved in a gel, as mentioned above.

Statistics. The data are presented as mean ± SEM. Statistical analysis was performed using Student's *t* test. In all the tests, we compared 2 groups and assumed a 2-tailed distribution and unequal variance. Values were considered significant at $P < 0.05$. The statistical tests for microarray analysis are described in Supplemental Methods.

Study approval. All experiments involving animals were reviewed and approved by the Veterinary Office of the Canton Vaud (SCA–EXPANIM, Service de la Consommation et des Affaires Vétérinaires, Epalinges, Switzerland) in accordance with the Federal Swiss Veterinary Office Guidelines. The utilization of human islets was approved by the Comité d'Ethique de la Recherche sur les Sujets Humains, CRCHUM.

Acknowledgments

We would like to thank B. Polat, J. Kocher, and B. Bordier for their help with histology and H. Mottaz for her help with genotyping. We thank Liliane Michalik and Nicolas Rotman for reading the manuscript and for their comments and Nathalie Constantin for her help in preparing the manuscript. This work was supported by the Swiss National Science Foundation (W. Wahli, B. Thorens, and P. Herrera), and the National Research Center "Frontiers in Genetics" (W. Wahli, B. Thorens, and P. Herrera), the Bonizzi-Theler-Stiftung (W. Wahli), the 7th EU program TORNADO (W. Wahli), and the Canadian Institute of Health Research and the Canadian Diabetes Association (M. Prentki). G.A. Rutter thanks the Wellcome Trust (programme grant 081958/Z/07/Z), MRC (G0401641), the NIH (ROI DKO71962-01), Diabetes UK, and the European Union FP6 ("SaveBeta") for grant support. B. Thorens and G.A. Rutter received support from the EU IMI FP7 program IMIDIA. A. Yessoufou received a scholarship from the Islamic Development Bank.

Received for publication June 5, 2012, and accepted in revised form July 19, 2012.

Address correspondence to: Walter Wahli, Center for Integrative Genomics, University of Lausanne, Le Génopode, CH-1015 Lausanne, Switzerland. Phone: 41.21.692.41.10; Fax: 41.21.692.41.15; E-mail: Walter.Wahli@unil.ch.

1. Lyssenko V, Groop L. Genome-wide association study for type 2 diabetes: clinical applications. *Curr Opin Lipidol*. 2009;20(2):87–91.
2. Nolan CJ, Damm P, Prentki M. Type 2 diabetes across generations: from pathophysiology to prevention and management. *Lancet*. 2011;378(9786):169–181.
3. Dor Y, Brown J, Martinez OI, Melton DA. Adult pancreatic beta-cells are formed by self-duplication rather than stem-cell differentiation. *Nature*. 2004;429(6987):41–46.
4. Inada A, et al. Carbonic anhydrase II-positive pancreatic cells are progenitors for both endocrine and exocrine pancreas after birth. *Proc Natl Acad Sci U S A*. 2008;105(50):19915–19919.
5. Rutter G. Nutrient-secretion coupling in the pancreatic islet beta-cell: recent advances. *Mol Aspects Med*. 2001;22(6):247–284.
6. Pørksen N, Hollingdal M, Juhl C, Butler P, Veldhuis JD, Schmitz O. Pulsatile insulin secretion: detection, regulation, and role in diabetes. *Diabetes*. 2002; 51(suppl 1):S245–S254.
7. Cerasi E, Ependic S, Luft R. Dose-response relation between plasma-insulin and blood-glucose levels during oral glucose loads in prediabetic and diabetic subjects. *Lancet*. 1973;1(7807):794–797.
8. Pørksen N. The in vivo regulation of pulsatile insulin secretion. *Diabetologia*. 2002;45(1):3–20.
9. Shibasaki T, et al. Essential role of Epac2/Rap1 signaling in regulation of insulin granule dynamics by cAMP. *Proc Natl Acad Sci U S A*. 2007; 104(49):19333–19338.
10. Rorsman P, Renström E. Insulin granule dynamics in pancreatic beta cells. *Diabetologia*. 2003; 46(8):1029–1045.
11. Kwan EP, et al. Munc13-1 deficiency reduces insulin secretion and causes abnormal glucose tolerance. *Diabetes*. 2006;55(5):1421–1429.
12. Schonn JS, et al. Rab3 proteins involved in vesicle biogenesis and priming in embryonic mouse chromaffin cells. *Traffic*. 2010;11(11):1415–1428.
13. Ivarsson R, Jing X, Waselle L, Regazzi R, Renström E. Myosin 5a controls insulin granule recruitment during late-phase secretion. *Traffic*. 2005; 6(11):1027–1035.
14. Wang Z, Thurmond DC. Differential phosphorylation of RhoGDI mediates the distinct cycling of Cdc42 and Rac1 to regulate second-phase insulin secretion. *J Biol Chem*. 2010;285(9):6186–6197.
15. Wang Z, Oh E, Thurmond DC. Glucose-stimulated Cdc42 signaling is essential for the second phase of insulin secretion. *J Biol Chem*. 2007; 282(13):9536–9546.
16. Wang Z, Thurmond DC. Mechanisms of biphasic insulin-granule exocytosis - roles of the cytoskeleton, small GTPases and SNARE proteins. *J Cell Sci*. 2009;122(pt 7):893–903.
17. Sumara G, et al. Regulation of PKD by the MAPK p38delta in insulin secretion and glucose homeostasis. *Cell*. 2009;136(2):235–248.
18. Poitout V, Robertson RP. Glucolipotoxicity: fuel excess and beta-cell dysfunction. *Endocr Rev*. 2008; 29(3):351–366.
19. Prentki M, Madiraju SR. Glycerolipid/free fatty acid cycle and islet beta-cell function in health, obesity and diabetes. *Mol Cell Endocrinol*. 2012; 353(1–2):88–100.
20. Itoh Y, et al. Free fatty acids regulate insulin secretion from pancreatic beta cells through GPR40. *Nature*. 2003;422(6928):173–176.
21. Gremlich S, et al. Pancreatic islet adaptation to fasting is dependent on peroxisome proliferator-activated receptor alpha transcriptional up-regulation of fatty acid oxidation. *Endocrinology*. 2005; 146(1):375–382.
22. Gupta D, Jetton TL, Mortensen RM, Duan SZ,

Peshavaria M, Leahy JL. In vivo and in vitro studies of a functional peroxisome proliferator-activated receptor gamma response element in the mouse pdx-1 promoter. *J Biol Chem*. 2008;283(47):32462–32470.
23. Cohen G, et al. Role of lipid peroxidation and PPAR-delta in amplifying glucose-stimulated insulin secretion. *Diabetes*. 2011;60(11):2830–2842.
24. Braissant O, Wahli W. Differential expression of peroxisome proliferator-activated receptor-alpha, -beta, and -gamma during rat embryonic development. *Endocrinology*. 1998;139(6):2748–2754.
25. Braissant O, Foufelle F, Scotto C, Dauça M, Wahli W. Differential expression of peroxisome proliferator-activated receptors (PPARs): tissue distribution of PPAR-alpha, -beta, and -gamma in the adult rat. *Endocrinology*. 1996;137(1):354–366.
26. Di-Poï N, et al. Epithelium-mesenchyme interactions control the activity of peroxisome proliferator-activated receptor beta/delta during hair follicle development. *Mol Cell Biol*. 2005;25(5):1696–1712.
27. Tan N, Icre G, Montagner A, Bordier-ten-Heggeler B, Wahli W, Michalik L. The nuclear hormone receptor peroxisome proliferator-activated receptor beta/delta potentiates cell chemotactism, polarization, and migration. *Mol Cell Biol*. 2007; 27(20):7161–7175.
28. Varnat F, et al. PPARbeta/delta regulates paneth cell differentiation via controlling the hedgehog signaling pathway. *Gastroenterology*. 2006;131(2):538–553.
29. Kostadinova R, Wahli W, Michalik L. PPARs in diseases: control mechanisms of inflammation. *Curr Med Chem*. 2005;12(25):2995–3009.
30. Michalik L, Wahli W. PPARs mediate lipid signaling in inflammation and cancer. *PPAR Res*. 2008; 2008:134059.
31. Riserus U, et al. Activation of peroxisome proliferator-activated receptor (PPAR)delta promotes reversal of multiple metabolic abnormalities, reduces oxidative stress, and increases fatty acid oxidation in moderately obese men. *Diabetes*. 2008;57(2):332–339.
32. Oliver WR Jr, et al. A selective peroxisome proliferator-activated receptor delta agonist promotes reverse cholesterol transport. *Proc Natl Acad Sci U S A*. 2001;98(9):5306–5311.
33. Serrano-Marco L, et al. Activation of Peroxisome Proliferator-Activated Receptor-{beta}/-{delta} (PPAR-{beta}/-{delta}) ameliorates insulin signaling and reduces SOCS3 levels by inhibiting STAT3 in Interleukin-6-stimulated adipocytes. *Diabetes*. 2011; 60(7):1990–1999.
34. Wang Y, et al. Peroxisome-proliferator-activated receptor delta activates fat metabolism to prevent obesity. *Cell*. 2003;113(2):159–170.
35. Schuler M, et al. PGC1alpha expression is controlled in skeletal muscles by PPARbeta, whose ablation results in fiber-type switching, obesity, and type 2 diabetes. *Cell Metab*. 2006;4(5):407–414.
36. Wan J, Jiang L, Lu Q, Ke L, Li X, Tong N. Activation of PPARdelta up-regulates fatty acid oxidation and energy uncoupling genes of mitochondria and reduces palmitate-induced apoptosis in pancreatic beta-cells. *Biochem Biophys Res Commun*. 2010; 391(3):1567–1572.
37. Ravnskjaer K, Frigerio F, Boergesen M, Nielsen T, Maechler P, Mandrup S. PPAR{delta} is a fatty acid sensor, which enhances mitochondrial oxidation in insulin-secreting cells and protects against fatty acid induced dysfunction. *J Lipid Res*. 2010; 51(6):1370–1379.
38. Bonal C, Thorel F, Ait-Lounis A, Reith W, Trumpp A, Herrera PL. Pancreatic inactivation of c-Myc decreases acinar mass and transdifferentiates acinar cells into adipocytes in mice. *Gastroenterology*. 2009; 136(1):309–319.
39. Zhang X, Gaspard JP, Mizukami Y, Li J, Graeme-Cook F, Chung DC. Overexpression of cyclin D1 in pancreatic beta-cells in vivo results in islet hyperplasia without hypoglycemia. *Diabetes*. 2005; 54(3):712–719.
40. Nguyen KT, et al. Essential role of Pten in body size determination and pancreatic beta-cell homeostasis in vivo. *Mol Cell Biol*. 2006;26(12):4511–4518.
41. Kang K, et al. Adipocyte-derived Th2 cytokines and myeloid PPARdelta regulate macrophage polarization and insulin sensitivity. *Cell Metab*. 2008; 7(6):485–495.
42. Odegaard J, et al. Alternative M2 activation of Kupffer cells by PPARdelta ameliorates obesity-induced insulin resistance. *Cell Metab*. 2008; 7(6):496–507.
43. Arribas M, Regazzi R, Garcia E, Wollheim CB, De Camilli P. The stimulatory effect of rabphilin 3a on regulated exocytosis from insulin-secreting cells does not require an association-dissociation cycle with membranes mediated by Rab 3. *Eur J Cell Biol*. 1997;74(3):209–216.
44. Schluter OM, Khvotchev M, Jahn R, Sudhof TC. Localization versus function of Rab3 proteins. Evidence for a common regulatory role in controlling fusion. *J Biol Chem*. 2002;277(43):40919–40929.
45. Springett GM, Kawasaki H, Spriggs DR. Non-kinase second-messenger signaling: new pathways with new promise. *Bioessays*. 2004;26(7):730–738.
46. Thurmond D, Gonelle-Gispert C, Furukawa M, Halban PA, Pessin JE. Glucose-stimulated insulin secretion is coupled to the interaction of actin with the t-SNARE (target membrane soluble N-ethylmaleimide-sensitive factor attachment protein receptor protein) complex. *Mol Endocrinol*. 2003;17(4):732–742.
47. Tsuboi T, da Silva Xavier G, Leclerc I, Rutter GA. 5′-AMP-activated protein kinase controls insulin-containing secretory vesicle dynamics. *J Biol Chem*. 2003;278(52):52042–52051.
48. Nevins A, Thurmond DC. Glucose regulates the cortical actin network through modulation of Cdc42 cycling to stimulate insulin secretion. *Am J Physiol Cell Physiol*. 2003;285(3):C698–C710.
49. Bard F, Malhotra V. The formation of TGN-to-plasma-membrane transport carriers. *Annu Rev Cell Dev Biol*. 2006;22:439–455.
50. Hausser A, Storz P, Martens S, Link G, Toker A, Pfizenmaier K. Protein kinase D regulates vesicular transport by phosphorylating and activating phosphatidylinositol-4 kinase IIIbeta at the Golgi complex. *Nat Cell Biol*. 2005;7(9):880–886.
51. Scaglia L, Cahill CJ, Finegood DT, Bonner-Weir S. Apoptosis participates in the remodeling of the endocrine pancreas in the neonatal rat. *Endocrinology*. 1997;138(4):1736–1741.
52. Rachdi L, et al. Differential effects of p27 in regulation of beta-cell mass during development, neonatal period, and adult life. *Diabetes*. 2006; 55(12):3520–3528.
53. Joberty G, Stabila PF, Coppola T, Macara IG, Regazzi R. High affinity Rab3 binding is dispensable for Rabphilin-dependent potentiation of stimulated secretion. *J Cell Sci*. 1999;112(pt 20):3579–3587.
54. Mosedale M, Egodage S, Calma RC, Chi NW, Chessler SD. Neurexin-1alpha contributes to insulin-containing secretory granule docking. *J Biol Chem*. 2012;287(9):6350–6361.
55. Olofsson C, et al. Impaired insulin exocytosis in NCAM-/- mice due to defective reorganization of the submembrane F-actin network. *Endocrinology*. 2009;150(7):3067–3075.
56. Li J, O'Connor KL, Hellmich MR, Greeley GH Jr, Townsend CM Jr, Evers BM. The role of protein kinase D in neurotensin secretion mediated by protein kinase C-alpha/-delta and Rho/Rho kinase. *J Biol Chem*. 2004;279(27):28466–28474.
57. Soriano P. Generalized lacZ expression with the ROSA26 Cre reporter strain. *Nat Genet*. 1999; 21(1):70–71.
58. Gao N, White P, Doliba N, Golson ML, Matschinsky FM, Kaestner KH. Foxa2 controls vesicle docking and insulin secretion in mature Beta cells. *Cell Metab*. 2007;6(4):267–279.
59. Reimann F, Habib AM, Tolhurst G, Parker HE, Rogers GJ, Gribble FM. Glucose sensing in L cells: a primary cell study. *Cell Metab*. 2008; 8(6):532–539.